ACS APPLIED BIO MATERIALS Cite This: ACS Appl. Bio Mater. 2018, 1, 1019−1027 Article www.acsabm.org

Biocompatible G-Quadruplex/Hemin for Enhancing Antibacterial Activity of H_2O_2

Yuqian Xing,[†] Xiao Liu,[†] Qinqin Pu,[‡] Min Wu,*[,‡] and Julia Xiaojun Zhao*[,†]

[†]Department of Chemistry, University of North Dakota, Grand Forks, North Dakota 58202, United States

[‡]Department of Biomedical Sciences, School of Medicine and Health Sciences, University of North Dakota, Grand Forks, North Dakota 58202, United States

Supporting Information

ABSTRACT: The G-quadruplex/hemin (G/H) complex has been broadly used in the field of bioanalytical chemistry for peroxidase-mimicking applications. The property of the G/H complex makes it possible to catalyze the decomposition of H_2O_2. The hydroxyl radical (·OH) generated during the procedure has a higher antibacterial performance than the original H_2O_2. Herein, an efficient and biocompatible antibacterial system, which provides the same antibacterial efficiency at lower H_2O_2 concentration to alleviate the H_2O_2 toxicity, has been demonstrated based on the conversion of H_2O_2 to ·OH. With the G/H complex as the additive, the antibacterial activity of H_2O_2 was vastly enhanced against both Gram-positive and Gram-negative bacteria in *in vitro* experiments. Furthermore, the designed antibacterial system was applied on the mice wound model *in vivo* and showed outstanding antibacterial activity of the G/H complex to prevent wound infection and facilitate wound healing. Our study renders the possibility of using the G/H complex to help control both Gram-positive and Gram-negative infections.

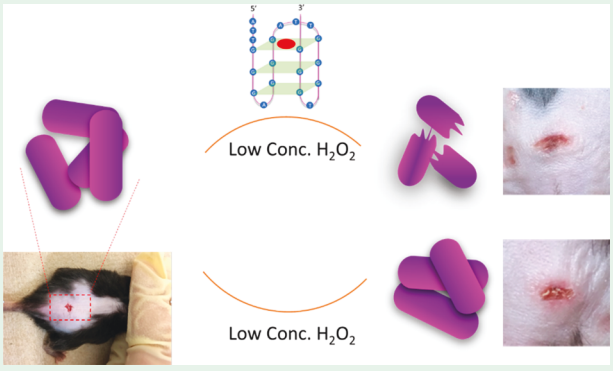

KEYWORDS: *G-quadruplex, DNAzyme, antibacterial, peroxidase-mimic activity, wound disinfection*

1. INTRODUCTION

Pathogenic bacteria are a major threat to human health worldwide.[1,2] To prevent bacterial infections, a number of antibacterial substances have been developed and are widely used in our daily life.[3] A variety of antiseptics,[4] such as antibiotics,[5] metal ions,[2] quaternary ammonium compounds,[6] and polymers,[7] have been tested and applied to prevent or treat bacterial infections through diverse antibacterial mechanisms. However, continued use of many antibacterial agents may decrease their effectiveness over time due to the emergency of drug-resistant bacterial strains.[5−9] Therefore, the development of new and powerful antibacterial agents is in critical need. In the past decade, the emerging field of nanoscience and nanotechnology has produced a number of novel nanomaterials that showed excellent antibacterial activity, such as silver nanoparticles,[2,10] carbon nanotubes,[11,12] graphene, and graphene-based nanomaterials.[12−14] In addition to the development of new antibacterial agents, improving the efficiency of existing antiseptics is also an attractive strategy due to low side effects, which would be an important consideration for new antimicrobial development.

One of the traditional disinfectant agents that is widely used is hydrogen peroxide (H_2O_2) solution, as its applications can range from wound treatment and sterilization to high-level disinfection for healthcare settings, etc.[15] Meanwhile, as a low cost surface disinfectant, H_2O_2 can also be used to sterilize semicritical and noncritical equipment due to its broad-spectrum bactericidal, virucidal, sporicidal, and fungicidal properties, excellent stability, and environmentally friendly characteristics. Usually, to achieve a desired disinfection efficiency, a high concentration of H_2O_2 is needed. For example, in a regular wound treatment, 0.5 to 3%, ca. 166 mM to 1 M H_2O_2[15,16] is needed to achieve the desired effectiveness, while in pharmaceutical and health care environments up to 35% of H_2O_2 is needed.[17] However, such a high concentration of H_2O_2 is harmful to human health. Thus, great caution is required during these application processes. Additionally, in the case of wound treatment, a high concentration of H_2O_2 could delay wound healing. Thus, a challenge for traditional antibacterial agent H_2O_2 remains, that is, how to keep its antibacterial efficiency with minimal amount of H_2O_2.

Recent research found that the antibacterial capacity of the hydroxyl radical (·OH) is much stronger than that of H_2O_2.[18] This finding provides a viable approach of using low concentration of H_2O_2 to enhance antibacterial effects if H_2O_2 could be converted to ·OH. In fact, two common

Received: June 8, 2018
Accepted: September 10, 2018
Published: September 10, 2018

DOI: 10.1021/acsabm.8b00211
ACS Appl. Bio Mater. 2018, 1, 1019−1027

approaches have been reported to convert H_2O_2 to ·OH. One is the indirect formation of ·OH from H_2O_2 via the iron-driven Fenton's reagent, a ferrous ion that catalyzes the decomposition of H_2O_2 to form ·OH.[19] This method has been widely used for wastewater treatment and hazardous chemical destruction.[20,21] The other method of converting H_2O_2 to ·OH is use of a peroxidase, such as catalase,[22] horseradish peroxidase,[23] and cytochrome c peroxidase.[24] Recently, nanomaterials with peroxidase-mimic property also played an important role for converting H_2O_2 to ·OH, which can significantly enhance the antibacterial property of H_2O_2.[25−27] Sun and co-workers have demonstrated that graphene quantum dots (GQDs) with peroxidase-like property displayed a strong enhancement of antibacterial activity of H_2O_2 against both Gram-negative (*Escherichia coli*) and Gram-positive (*Staphylococcus aureus*) bacteria.[25] Gao and co-workers have reported that ferromagnetic nanoparticles with peroxidase-like activity can enhance antibacterial activity in the presence of H_2O_2 at the concentration of 1%.[27] However, the iron ions and those nanomaterials are potentially toxic to healthy cells.[27−29] Moreover, the synthetic procedures are complex and difficult to scale up.

To overcome these challenges, we proposed to use DNAzymes to convert H_2O_2 to ·OH.[30−32] DNAzymes with peroxidase-like activity were first reported in the late 1990s.[33,34] Essentially, as a class of DNAzymes, G-quadruplex/hemin (G/H) complexes are hemin molecules bonded with their guanine-rich single strand DNA (ssDNA) aptamers, forming a quadruplex structure with the hydrogen bond between guanine bases.[34−36] This artificial system would increase the catalytic activity of hemin.[34] Up to recently, the G/H complex with peroxidase-like activity was mainly applied in bioanalytical chemistry for biosensing.[37−43] In addition, the G/H complex was also applied *in vitro*.[44,45] Zhang and co-workers used nanogel as a carrier to deliver the G/H complex into cells for selective oxidation.[44] However, the applications of the G/H complex for converting H_2O_2 to ·OH, as well as for antibacterial researches, have not been reported.

Our design combined the advantages of oligonucleotides, such as thermal stability, hydrolysis resistance, ease of synthesis and modification, potential for scale production,[46] and excellent peroxidase-mimic property. An antibacterial system based on a low concentration of H_2O_2 and the G/H complex as the additive was designed. The results showed that the addition of the G/H complex could effectively enhance the antibacterial activity against representatives of both Gram-positive and Gram-negative bacteria and dramatically inhibit their growth. The developed complex was successfully applied to the *in vivo* wound disinfection model without apparent side effects.

2. EXPERIMENTAL SECTION

2.1. Materials. Hydrogen peroxide (≥30.0%), terephthalic acid (TA), 2,2′-azinobis(3-ethylbenzthiazoline-6-sulfonate) (ABTS), potassium chloride (ACS reagent, ≥99.0%), dimethyl sulfoxide (DMSO), ethylenediaminetetraacetic acid (EDTA), hemin, 2-amino-2-(hydroxymethyl)-1,3-propanediol (Tris-base), 3-(4,5-dimethyl-2-thiazolyl)-2,5-diphenyltetrazolium bromide (MTT), and 5,5-dimethyl-1-pyrroline *N*-oxide (DMPO) were purchased from Sigma-Aldrich Inc. Roswell Park Memorial Institute (RPMI) medium 1640, Lysogeny broth (LB) medium, fetal bovine serum (FBS), 4′-6-diamidino-2-phenylindole (DAPI), and propidium iodide (PI) were purchased from Thermo Fisher Scientific Inc. The deionized (DI) water (18.2 MΩ·cm) was produced from a Millipore water purification system. Male C57BL/6 mice of 6−8 weeks old were purchased from Charles River. *E. coli* O157:H7 strain (ATCC 43888), *S. aureus* strain (ATCC 13301), and the macrophage cell line (MH-S) were obtained from the American Tissue Culture Collection (ATCC). The colon cancer cell line (SW620) was provided by MD Anderson Cancer Center.[47] All experiments involved in animals were approved by the Institutional Animal Care and Use Committee (IACUC) in University of North Dakota. All oligonucleotides were synthesized by IDT Inc. The G-quadruplex sequence was B7−3−0 (5′- ATT GGG AGG GAT TGG GTG GG-3′).[48]

2.2. Instruments. UV−vis absorption measurements were performed on a PerkinElmer Lambda 1050 UV/vis/NIR spectrometer (PerkinElmer, Santa Clara, CA), equipped with a Peltier temperature control accessory. Fluorescence intensities were measured using a Horiba Fluorolog-3 spectrofluorometer. The fluorescence images were taken using a Nikon Eclipse 80i (upright) fluorescence microscope. A Hitachi SU8010 field emission scanning electron microscope (SEM) was used to take the SEM images of the H_2O_2-treated bacteria. The optical density (OD) values of sample solution for MTT assays were measured at 560 nm using a multiskan spectrum spectrophotometer (Thermofisher Scientific, Waltham, MA).

2.3. Preparation of DNAzyme. Hemin solution (4.0 mM) was first dissolved in 5 mL of DMSO as the stock solution. The oligonucleotide of 100 nmol was dissolved in 1 mL of Tris-EDTA (TE) buffer and stored at −20 °C. An aliquot of 200 μL of obtained oligonucleotide solution was heated to 95 °C and was kept at this temperature for 5 min and then cooled to room temperature and remained for 60 min to dissociate any intermolecular interactions. Subsequently, an aliquot of 5 μL of 0.1 M KCl solution was added to the oligonucleotide solution and was incubated at room temperature for 40 min. Finally, an aliquot of 2.6 μL of hemin stock solution was added up to a concentration of 50 μM and was incubated at room temperature for 60 min. The formed G/H complexes were diluted to required concentrations using Tris−HCl buffer (25 mM, pH 6.8) prior to usage.

2.4. Culture of Bacteria and Detection of Antibacterial Activity of the Developed Reagents. Monocolony bacteria of *E. coli* and *S. aureus* were cultured in the LB medium and shaken at 37 °C overnight before usage.[49] The bacterial cells were collected by centrifuging and redispersed in Tris−HCl buffer with an optical density of 1 at 600 nm (OD_{600}).[50] Then, the bacteria were diluted to 10^6 CFU mL^{-1} using a sterile Tris−HCl buffer. The as-prepared bacterial solution was mixed with different concentrations of G/H complex and H_2O_2, incubating at 37 °C for 30 min under shaking. Then, an aliquot of 100 μL of the bacterial suspension was added into 900 μL of LB medium for growth in a shaking incubator at 37 °C overnight. The concentration of bacteria was finally determined by counting the numbers of bacterial colonies on plates.[51]

2.5. Study of the Cell Wall/Membrane Integrity. An aliquot of 20.0 μL of log phase *E. coli* (10^9 CFU mL^{-1}) cells was dispersed in 200 μL of Tris−HCl buffer with or without 1 μL of 0.2 mM G/H complex. After incubation for 2 h at 37 °C, the bacteria were stained with 200 μL of DAPI (12.50 μg/mL) and PI (1.25 μg/mL) for 15 min under the dark.[52] Then the collected cells were imaged using a Nikon Eclipse 80i (upright) fluorescence microscope.

2.6. *In Vivo* Mouse Wound Model. A mouse wound model[25,26] was used to evaluate the anti-infection efficiency of H_2O_2 in the G/H complex *in vivo*. A total of 15 male mice with about 4 mm^2 wound area were divided into five groups to be treated with different solutions: 0.1 M H_2O_2, saline, 1 μM G/H complex, 1 mM H_2O_2, and 1 mM H_2O_2 + 1 μM G/H complex. After a wound was created, an aliquot of 50 μL of *S. aureus* (1×10^8 CFU/mL) was first placed on the wound area, followed by covering with an absorbent wound dressing infused with 50 μL of different solutions, respectively. The reagents were added every 24 h, and the photos of the wound area of each mouse were taken. After 72 h, the scabs of the wound were harvested and kept in PBS buffer. The numbers of bacteria were quantified by counting the colonies on the agar plate.

DOI: 10.1021/acsabm.8b00211
ACS Appl. Bio Mater. 2018, 1, 1019−1027

2.7. Cytotoxicity of G/H Complex Used As Additive. The bacteria *E. coli* and *S. aureus* were seeded in 96-well plates and treated with various concentrations of the G/H complex at 37 °C for 5 h. Then, each well was added by 10 μL of 5 mg/mL MTT reagent to form the purple products after 4 h, followed by adding 100 μL of DMSO solution to stop the reaction and dissolve the precipitant thoroughly.[53] The absorption of each well at 570 nm was recorded to determine the cell survival rate.

SW620 cells and MH-S cells were cultured in 1640 medium supplemented with 10% FBS at 37 °C overnight.[47] Both cells were treated with various concentrations of the G/H complex at 37 °C for 24 h. Then, the MTT method was performed to determine cell viability.

2.8. Spin Trapping Technique Using Electron Paramagnetic Resonance for Detection of ·OH. Approximately 30 μL of sample was loaded into a borosilicate capillary tube (0.70 mm i.d./1.25 mm o.d.; VitroGlass, Inc.), which was mounted in a Varian E-109 spectrometer fitted with a cavity resonator. All continuous-wave (CW) EPR spectra were obtained with an observation power of 12.5 mW. All spectra were obtained with a modulation frequency of 100 kHz and a modulation amplitude of 1 G. The spin trap agent DMPO was used to capture the formed ·OH.

3. RESULTS AND DISCUSSIONS

3.1. Formation of a Hydroxyl Radical from H_2O_2 by G/H DNAzyme. The formation of ·OH through chemical decomposition of H_2O_2 catalyzed by G/H DNAzyme is the critical step in our design. So far, this reaction has not been demonstrated in the literature. In 2016, Cai and co-workers developed a fluorometric assay platform for the detection of caffeic acid based on the oxidation of the intermediate from decomposition of H_2O_2 catalyzed by G/H DNAzyme, but it was not proved whether the intermediate was ·OH or not.[54]

The challenge was how to accurately measure the produced ·OH in the reaction process. The lifetime of ·OH in solution is about 10^{-9} s, making it extremely difficult to be detected.[55] Based on the spin trapping technique, electron paramagnetic resonance (EPR) has been applied to detect ·OH.[56−58] As shown in Figure 1, a typical spectrum of DMPO−OH, which

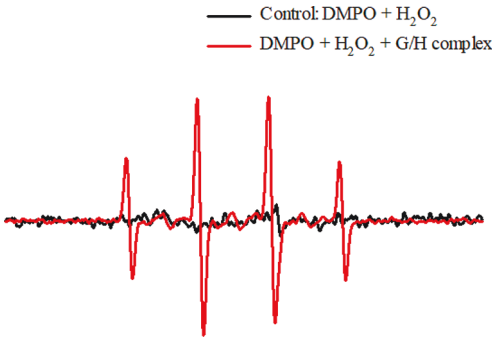

Figure 1. CW EPR spectra of DMPO−OH. Condtions: 10 mM H_2O_2, 25 μM G/H complex, 500 mM DMPO in 25 mM Tris-HCl buffer (pH 6.8), incubation at room temperature for 30 min. Signal average time is 20−25 min for each sample.

was in 1:2:2:1 quartet format,[56] was presented in the presence of the G/H complex. However, there was no distinctive or special spectrum for control without the G/H complex. Although EPR is only a semiquantitative approach for detecting ·OH, the result qualitatively confirmed the formation of ·OH during the reaction catalyzed by the G/H complex.

Meanwhile, an indirect method was performed to further demonstrate the formation of ·OH. According to the literature, the generated ·OH could be monitored using a fluorescence method in which TA could capture ·OH and generate fluorescent 2-hydroxy terephthalic acid (TAOH) with a fluorescence emission peak at 435 nm.[25,59,60] Based on this information, the TA might be an ideal probe for investigation of the formation of ·OH in a reaction. Thus, in this work, we adopted this fluorescence method to confirm the formation of ·OH. First, we prepared G/H DNAzyme as described in section 2.3. Then, to verify the generation of ·OH in the decomposition of H_2O_2, a series of fluorescence measurements were conducted using different solutions. The results were shown in Figure 2. When only TA existed in the solution, no

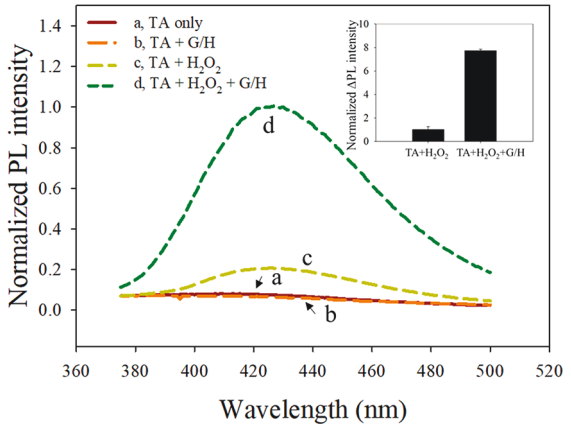

Figure 2. Normalized fluorescence spectra of TAOH formed under different conditions, including only TA (curve a); TA and G/H complex (curve b); TA and H_2O_2 (Curve c); and TA, H_2O_2, and G/H complex (curve d). Condtions: 20 mM PBS buffer (pH 7.4), incubation at room temperature for 12 h. The concentrations of TA, H_2O_2, and G/H complex were 0.5 mM, 1 mM, and 1 μM, respectively. λ_{ex}: 315 nm. λ_{em}: 435 nm. Inset: the normalized ΔPL intensity with or without the G/H complex.

fluorescence signals were observed (curve a). At this moment, the G/H complex was added to the TA solution. Still, no fluorescence signals were obtained (curve b). These results showed that both TA and the G/H complex are not fluorescence materials. In parallel, a TA solution containing H_2O_2 was detected (curve c). A small fluorescence peak at 435 nm was shown in curve c. The fluorescence peak indicated that the individual H_2O_2 can oxidize TA and release ·OH spontaneously. However, when the G/H complex was added as an additive, the fluorescence intensity increased dramatically (curve d). The comparison of fluorescence enhancement between curve c and d was shown in the inset of Figure 2. It was about an 8 times increase in intensity compared to the solution without the G/H complex. The results clearly demonstrated the ability of the G/H complex to convert H_2O_2 to ·OH.

3.2. Optimization of the Peroxidase-Mimic Activity of the G/H DNAzyme. In order to achieve the highest production efficiency of the ·OH radical, we optimized the peroxidase-mimic activity of the synthesized G/H complex. The G/H complex is a DNAzyme in which the hemin molecules bound with their guanine-rich single-stranded DNA (ssDNA) aptamers, forming a quadruplex structure with the hydrogen bond between guanine bases. Here, we first synthesized a G/H complex with a reported high peroxidase-mimic activity structure, B7−3−0.[41] The experimental

DOI: 10.1021/acsabm.8b00211
ACS Appl. Bio Mater. 2018, 1, 1019−1027

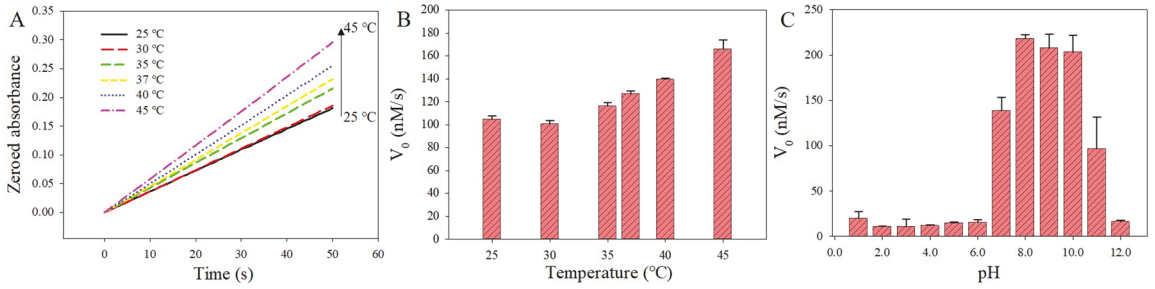

Figure 3. Optimization of peroxidase-mimic activity of G/H complex: (A) Plots of absorbance at 420 nm versus G/H complex at different temperatures. Experiments were performed using the 1 μM G/H complex and 1 mM H_2O_2 in 25 mM Tris-HCl buffer (pH 6.8) with 2 mM ABTS work solution at different temperatures. (B) V_0 values of the G/H complex at different temperatures. (C) V_0 values of the G/H complex at different pH. Experiments were performed using 1 μM G/H complex and 1 mM H_2O_2 in 2 mM ABTS working solution at 37 °C at different pH.

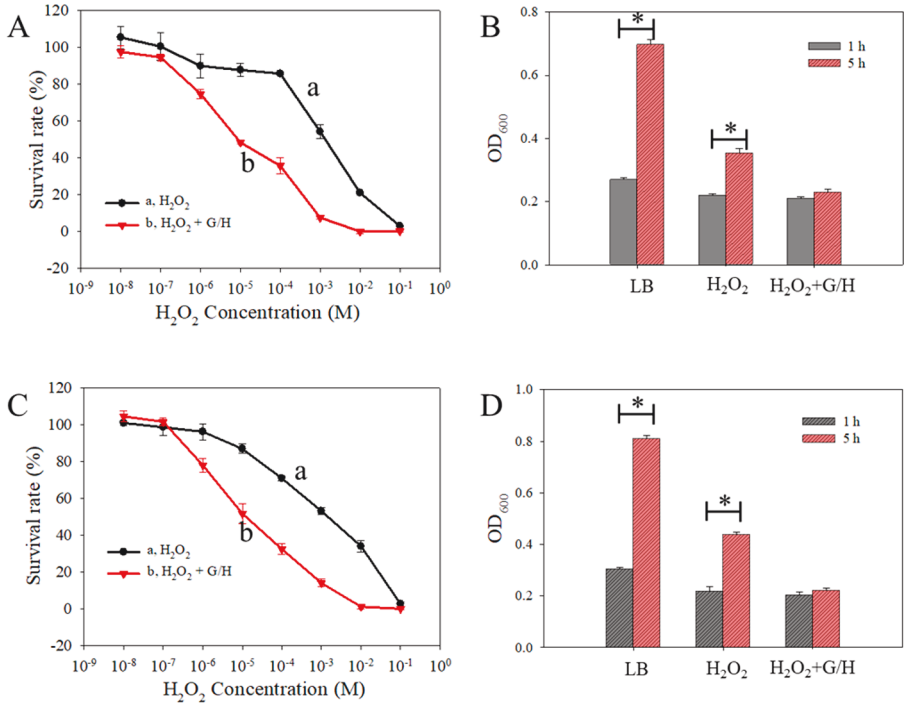

Figure 4. (A) Survival rate of *E. coli* treated with H_2O_2 at different concentration coincubation (10^{-8}, 10^{-7}, 10^{-6}, 10^{-5}, 10^{-4}, 10^{-3}, 10^{-2}, 10^{-1} M) with or without 1 μM G/H complex. Incubation at 37 °C for 30 min in Tris-HCl buffer. (B) Growth inhibition experiment by incubation in 0.01 M H_2O_2 with or without a 1 μM G/H complex at 37 °C in different medium solutions at 1 and 5 h. *p < 0.01. (C) and (D) for Gram-negative bacteria, *S. aureus*. The experimental conditions are similar to (A) and (B).

procedure was described in section 2.3. The peroxidase-mimic activity of the synthesized G/H complex was proved by catalytic oxidation of ABTS in the presence of H_2O_2. As shown in Figure S1A (Supporting Information), only the group with both H_2O_2 and G/H complex led to the color change from translucent green to dark green. This qualitatively demonstrated the peroxidase-mimic activity of the G/H complex. The result was also verified by UV−vis absorption at 420 nm (Figure S1B).

The peroxidase-like activity of the G/H complex was evaluated by the initial velocity V_0 of formed oxidized ABTS$^+$.[48,61,62] As shown in Figure 3A and 3B, the V_0 value increased from 104 nM/s at 25 °C with increasing temperature. The result was similar to the literature, describing that the G/H complex was thermophilic.[61] Considering the antibacterial applications to various biological samples, the temperature higher than 37 °C was not optimal. Herein, 37 °C was chosen as the working temperature. Besides temperature, the pH value also affected the oxidation extent significantly. As shown in Figure 3C, the V_0 value was very small in acidic conditions (pH 1.0−6.0). It showed large values in neutral pH to weak alkali conditions (pH 7.0−10.0). The optimal pH of the G/H complex was pH 8.0. Considering the small difference with optimum and application scenarios on skins, a Tris-HCl (pH 6.8) buffer was chosen as the reaction medium in the following work.

3.3. Enhanced Antibacterial Property of H_2O_2 by the G/H Complex. The G/H complex has demonstrated catalytic capacity on reduction of H_2O_2 to release the ·OH radical. Our objective is to enhance the antibacterial activity of H_2O_2. Next, using both Gram-negative bacteria *E. coli* and Gram-positive bacteria *S. aureus*, we investigated the ability of the G/H complex to facilitate antibacterial activity of H_2O_2. As shown in Figure 4A, the potency of pure H_2O_2 in killing *E. coli* was examined and was shown to be in a dose-dependent manner. The higher the concentration of H_2O_2 was, the lower the

DOI: 10.1021/acsabm.8b00211
ACS Appl. Bio Mater. 2018, 1, 1019−1027

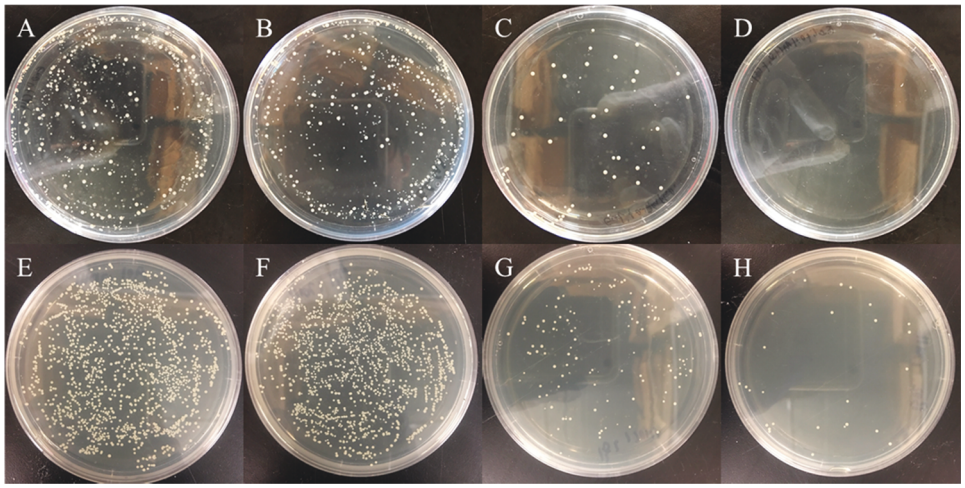

Figure 5. Representative photos of bacterial colonies showing the influences of the catalytic activity of the G/H complex on the growth of *E. coli.* (up) and *S. aureus* (bottom). (A and E) Bacterial cells only; (B and F) bacteria with 1 μM G/H complex; (C and G) bacteria with 0.01 M H_2O_2; (D and H) bacteria with 0.01 M H_2O_2 + 1 μM G/H complex. Incubation at 37 °C for 30 min.

bacterial survival rate was. As shown in Figure 4A curve a, the H_2O_2 concentration increased from 10^{-8} to 10^{-1} M, and the bacterial survival rate decreased from 100% to 0%. However, when the G/H complex was added, the bacterial viability significantly decreased compared to that without the G/H complex. As shown in Figure 4A curve b, a concentration of 1 mM H_2O_2 could reach 0% bacterial survival rate, while 0.1 M H_2O_2 was needed to achieve a similar effect for pure H_2O_2, 2 orders of magnitude lower, and is a relatively safe H_2O_2 concentration for clinical application.

The improved antibacterial activity was also demonstrated by inhibiting the growth of *E. coli* (Figure 4B). The same amount of *E. coli* was incubated in three cell culture media: the regular LB medium, the regular LB medium +0.01 M H_2O_2, and the regular LB medium +0.01 M H_2O_2 + 1 μM G/H complex. The bacterial concentration was measured by detection of OD_{600}. After 1 h of incubation, the *E. coli* concentration was 0.27 ± 0.01 (LB only), 0.22 ± 0.01 (LB + H_2O_2), and 0.21 ± 0.01 (LB + H_2O_2 + G/H complex) (Figure 4B, black columns). At this moment the bacterial concentration was comparable in these three media. Then, the culture time for the bacterial cells was extended to 5 h (Figure 4B, red columns). The bacterial concentration was increased to 0.70 ± 0.02 and 0.35 ± 0.02 in the regular LB medium and LB + H_2O_2 medium, respectively. However, in the LB +H_2O_2 + G/H complex medium, the bacterial growth was limited to 0.23 ± 0.01. The student *t* test showed a significant difference between the G/H complex group and these two control groups. These results indicated the bacterial cells were able to grow in the presence of 0.01 M H_2O_2. However, as the addition of the G/H complex presented, the growth of bacteria was greatly inhibited. Thus, the G/H complex improved the antibacterial activity of H_2O_2 for Gram-positive bacteria.

We further tested Gram-negative bacteria, *S. aureus*, using the same method. The results were shown in Figure 4C and D. Compared with Figure 4A and B, both the bacterial survival rate and the bacterial quantity are similar to the Gram-positive bacteria. Therefore, the G/H complex could be used to enhance the antibacterial activity of H_2O_2 for both Gram-negative and Gram-positive bacteria.

To visualize the above results, the antibacterial activity of the designed complex was further investigated using the CFU counting method. As shown in Figure 5, the top panel was *E. coli* cells, and the bottom panel was *S. aureus* cells. After being treated with 0.01 M H_2O_2 (Figure 5C and G), the bacterial colonies formed on the LB-agar plate were much less than the control groups (Figure 5A and E, B and F). However, when the bacteria groups were treated within the G/H complex +0.01 M H_2O_2 (D and H), the colony counts significantly reduced. Noticeably, there was no *E. coli* colony formed after treating with 0.01 M H_2O_2 and the 1 μM G/H complex (Figure 5D). This result further supported the concept that the G/H complex can enhance the antibacterial activity.

3.4. Effect of G/H Complex on Bacterial Cell Membrane Integrity. To further explore the antibacterial mechanism of G/H complex assisted H_2O_2, the bacterial cell wall/membrane integrity was examined using *E. coli* as an example bacterium. Two fluorescent molecules, DAPI and PI, were used to stain the *E. coli* cells. According to the literature,[63,64] DAPI can stain all cells, while PI can only stain membrane damaged cells. As shown in Figure 6(A), the bacteria without treatment showed a few red spots stained by PI, demonstrating that most of the bacterial cells were alive. The bacterial group treated with the G/H complex only (B) showed the similar results with group A. Only a few bacterial cells stained by PI indicated that there was no direct harm of the G/H complex on bacteria. After treating bacteria with 0.01 M H_2O_2 for 2 h (C), more cells were stained by the red color. Pink staining that indicates colocalization was observed in the merged image in addition to a number of DAPI only stained cells. In this condition, about half of the bacterial cells were killed by H_2O_2. Compared to these three control groups, in the presence of the G/H complex + H_2O_2 (Figure 6D), most of the *E. coli* cells were stained by both DAPI and PI, implying damage on the cell wall/membranes. Therefore, the existence of the G/H complex in the system facilitates the destruction of the bacteria cell wall/membrane.

Scanning electron microscopy was also used to directly observe the change of the bacterial cell wall/membrane after treating with different drug solutions. As shown in Figure 7, for two negative control groups treated with saline and G/H complex (Figure 7A and 7B), the *E. coli* cells were still in the ordinary rod shape, with relatively smooth cell walls. It demonstrated that the cells in these two groups were still

DOI: 10.1021/acsabm.8b00211
ACS Appl. Bio Mater. 2018, 1, 1019−1027

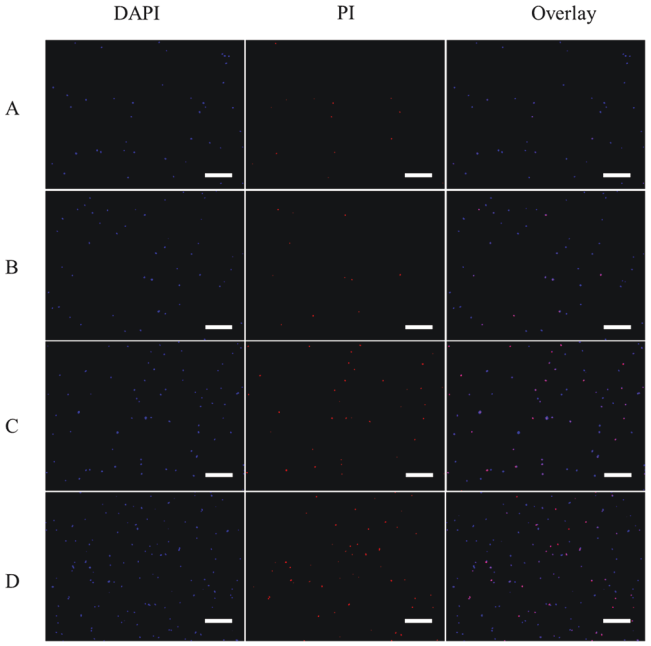

Figure 6. Fluorescence images of live and dead *E. coli* cells after incubation with 10 mM H_2O_2 for 2 h: (A) *E. coli* only; (B) *E. coli* with 1 μM of G/H complex; (C) *E. coli* with 0.01 M H_2O_2; (D) *E. coli* with 0.01 M H_2O_2 + 1 μM G/H complex. Blue fluorescence shows bacterial quasinuclear staining with DAPI, while red fluorescence shows dead bacteria staining with PI. Bar scale: 20 μm.

healthy. After treating with 0.01 M H_2O_2 (Figure 7C), the bacterial cell walls/membranes became unsmooth with some irregular asperities because of the H_2O_2 damage. Remarkably, after treating with the H_2O_2 + G/H complex (Figure 7D), the morphology of the whole cell wall became rough. To further confirm this result, we investigated the morphology change of *S. aureus* (Figure 7, bottom panel). The resulting SEM images were similar to that of *E. coli* (Figure 7E–H). Both bacterial SEM images demonstrated that the G/H complex could obviously enhance the antibacterial activity of H_2O_2. The enhancement manner was directly killing bacteria but through the additive G/H complex as an auxiliary.

3.5. Anti-Infection Effect of the G/H Complex on Wound Healing. To expand the antibacterial applications of the G/H complex *in vivo*, the anti-infection efficiency of the G/H complex was investigated using back-wounded mice as a model.[25,26,65] The wounds on the mice were artificially made under similar conditions. Then, *S. aureus* bacterial cells were placed on the wound to accelerate wound infection. Then, five groups of mice were treated with 0.1 M H_2O_2, saline, 1 μM G/H complex, 1 mM H_2O_2, and 1 μM G/H complex + 1 mM H_2O_2, respectively. Three mice in each group were used for parallel experiments. With a 24 h interval, new absorbent wound dressings infused with new treating solutions were covered on the wound, and the wound recovery processes were recorded by camera (Figure 8). The effective concentration of

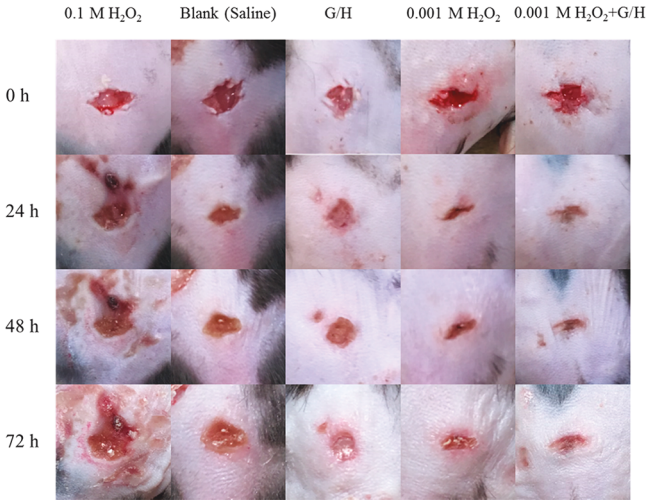

Figure 8. Photographs of wounds on mice treated with different solutions (0.1 M H_2O_2, saline, 1 μM G/H complex, 1 mM H_2O_2, 1 μM G/H complex + 1 mM H_2O_2) at indicated times.

H_2O_2 was 1 mM, which was much lower than the commercial H_2O_2 products (166 mM to 1 M) for wound disinfection. After treating the wounds with H_2O_2 + G/H complex for 72 h, the wounds on mice were almost fully healed without any erythema and edema. Although the wounds on mice in the 1 mM H_2O_2 group also healed significantly, the area around the wound was slightly red and swollen compared to the group treated with the H_2O_2 + G/H complex. Unlike the groups treated with H_2O_2, the wounds of mice in saline and the G/H complex group showed the regular inflammatory reaction during wound healing processes. Some erythema and edema were found during the 72 h treatment. This result demonstrated that the combination of the G/H complex

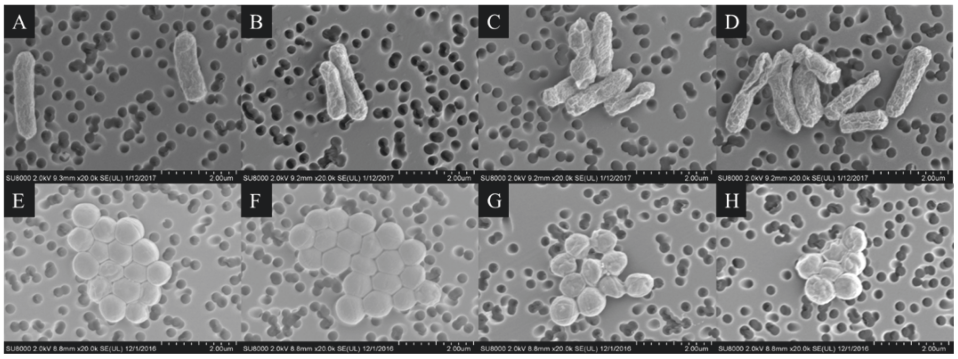

Figure 7. SEM images of bacterial morphology. (A) *E. coli*; (B) *E. coli* incubated with 1 μM G/H complex; (C) *E. coli* incubated with 0.01 M H_2O_2; (D) *E. coli* incubated with 0.01 M H_2O_2 and 1 μM G/H complex; (E) *S. aureus*; (F) *S. aureus* incubated with 1 μM G/H complex; (G) *S. aureus* incubated with 0.01 M H_2O_2; (H) *S. aureus* incubated with 0.01 M H_2O_2 and 1 μM G/H complex. Incubation at 37 °C for 30 min.

DOI: 10.1021/acsabm.8b00211
ACS Appl. Bio Mater. 2018, 1, 1019–1027

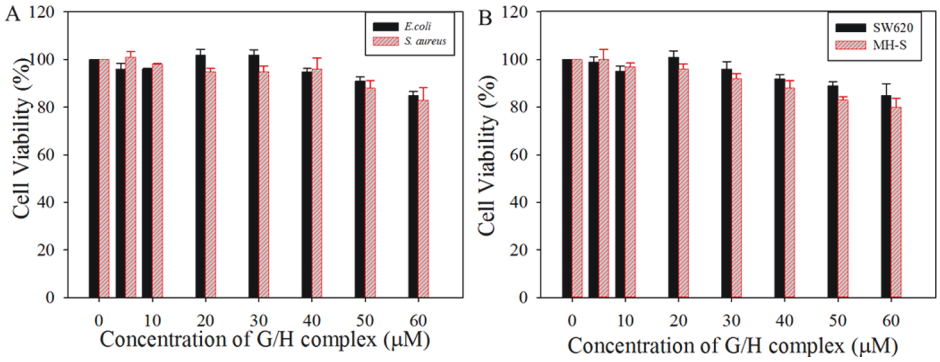

Figure 9. Relative cell viability of *E. coli* and *S. aureus* (A) and SW620 and MH-S (B) after culturing with different concentrations of G/H complex (0, 5, 10, 20, 30, 40, 50 to 60 μM). Incubatione conditions: 5 h for bacteria, 24 h for SW620 and MH-S at 37 °C.

with H_2O_2 could also play a role in resisting wound infection and accelerating wound healing *in vivo*. Additionally, the group treated with a relatively high level of H_2O_2 (0.1 M) showed a more adverse outcome on the skin. This concentration of H_2O_2 aggravated the damage of skin, rather than healing. Collectively, these findings illustrated the significance of reducing H_2O_2 concentration for wound healing.

3.6. Cytotoxicity Study of the G/H Complex. One of the main purposes of this work is to decrease the health tissue damage when using H_2O_2 as antiseptics. *In vitro* antibacterial experiments demonstrated that G/H itself was not harmful to bacteria (Figure 5B and F, Figure 7B and F). To further investigate the cytotoxicity of the G/H complex toward bacteria and mammalian cells, the MTT assay was performed. Two bacteria (*E. coli* and *S. aureus*) and two mammalian cell lines, a macrophage cell line (MH-S) and a colon cancer cell line (SW620), were used. The cell viabilities of bacteria and mammalian cell lines were measured after incubating with different concentrations of G/H complex for 5 and 24 h, respectively. As shown in Figure 9, for both bacteria and mammalian, almost 100% of the cells were still alive after incubation with the G/H complex in the range of 0 to 20 μM, which was about 20-fold higher than its working concentration. When the concentration went to a higher range (up to 60 μM), the cell survival rate started to decrease, but above 80%. This suggests a low intrinsic toxicity to cells at a high concentration, which is mostly derived from the toxicity of hemin.[66,67] However, there is no cytotoxicity of the G/H complex used as an additive at low concentrations, making the G/H complex a biocompatible agent for disinfection.

4. CONCLUSIONS

In conclusion, the G/H complex was designed and used as an additive to H_2O_2 to achieve the same antibacterial effect in a much lower dose of H_2O_2. By converting H_2O_2 into ·OH, higher antibacterial activity was achieved through catalyzing the decomposition of H_2O_2. Therefore, low concentrations of H_2O_2 can be used to kill bacteria with a high efficiency with little harmful effects to healthy tissues. The addition of the G/H complex showed excellent antibacterial properties against both Gram-negative (*E. coli*) and Gram-positive (*S. aureus*) bacteria *in vitro* without significant cytotoxicity. Furthermore, the G/H complex based antibacterial system also showed outstanding anti-infection property *in vivo* on a mouse wound model. Overall, the intrinsic properties of oligonucleotides made the G/H complex an ideal additive in industry.

■ ASSOCIATED CONTENT

Supporting Information

The Supporting Information is available free of charge on the ACS Publications website at DOI: 10.1021/acsabm.8b00211.

Colorimetric and UV−vis data of ABTS oxidization catalyzed by the G/H complex (PDF)

■ AUTHOR INFORMATION

Corresponding Authors

*E-mail: julia.zhao@und.edu.

*E-mail: min.wu@med.und.edu.

ORCID

Julia Xiaojun Zhao: 0000-0002-9603-666X

Notes

The authors declare no competing financial interest.

■ ACKNOWLEDGMENTS

We would like to thank Prof. Zhongyu Yang and Dr. Yanxiong Pan from the North Dakota State University for their great help with performing the spin trapping experiment using an electron paramagnetic resonance instrument in their lab for detection of ·OH. This work was supported by National Science Foundation Grant CHE 1709160 and the North Dakota Industrial Commission Grant G-041-081. NIH AI101973-01, AI109317-01A1, AI097532-01A1 to MW, and the University of North Dakota Core Facilities were supported by NIH grants INBRE P20GM103442, COBRE P30GM103329, and COBRE P20GM113123.

■ REFERENCES

(1) Rizzello, L.; Pompa, P. P. Nanosilver-Based Antibacterial Drugs and Devices: Mechanisms, Methodological Drawbacks, and Guidelines. *Chem. Soc. Rev.* **2014**, *43*, 1501−1518.

(2) Marambio-Jones, C.; Hoek, E. M. V. A Review of the Antibacterial Effects of Silver Nanomaterials and Potential Implications for Human Health and the Environment. *J. Nanopart. Res.* **2010**, *12*, 1531−1551.

(3) Williamson, D. A.; Carter, G. P.; Howden, B. P. Current and Emerging Topical Antibacterials and Antiseptics: Agents, Action, and Resistance Patterns. *Clin. Microbiol. Rev.* **2017**, *30*, 827−860.

(4) Dissemond, J.; Augustin, M.; Eming, S. A.; Goerge, T.; Horn, T.; Karrer, S.; Schumann, H.; Stucker, M. Modern Wound Care - Practical Aspects of Non-Interventional Topical Treatment of Patients with Chronic Wounds. *J. Dtsch. Dermatol. Ges.* **2014**, *12*, 541−554.

(5) Levy, S. B.; Marshall, B. Antibacterial Resistance Worldwide: Causes, Challenges and Responses. *Nat. Med.* **2004**, *10*, 122−129.

DOI: 10.1021/acsabm.8b00211
ACS Appl. Bio Mater. 2018, 1, 1019−1027

(6) Buffet-Bataillon, S.; Tattevin, P.; Bonnaure-Mallet, M.; Jolivet-Gougeon, A. Emergence of Resistance to Antibacterial Agents: the Role of Quaternary Ammonium Compounds–a Critical Review. *Int. J. Antimicrob. Agents* **2012**, *39*, 381−389.
(7) Eberlein, T.; Assadian, O. Clinical Use of Polihexanide on Acute and Chronic Wounds for Antisepsis and Decontamination. *Skin Pharmacol. Physiol.* **2010**, *23*, 45−51.
(8) Chernousova, S.; Epple, M. Silver as Antibacterial Agent: Ion, Nanoparticle, and Metal. *Angew. Chem., Int. Ed.* **2013**, *52*, 1636−1653.
(9) Payne, D. J.; Gwynn, M. N.; Holmes, D. J.; Pompliano, D. L. Drugs for Bad Bugs: Confronting the Challenges of Antibacterial Discovery. *Nat. Rev. Drug Discovery* **2007**, *6*, 29−40.
(10) Kim, K. J.; Sung, W. S.; Suh, B. K.; Moon, S. K.; Choi, J. S.; Kim, J. G.; Lee, D. G. Antifungal Activity and Mode of Action of Silver Nano-Particles on Candida Albicans. *BioMetals* **2009**, *22*, 235−242.
(11) Kang, S.; Pinault, M.; Pfefferle, L. D.; Elimelech, M. Single-Walled Carbon Nanotubes Exhibit Strong Antimicrobial Activity. *Langmuir* **2007**, *23*, 8670−8673.
(12) Wu, M. C.; Deokar, A. R.; Liao, J. H.; Shih, P. Y.; Ling, Y. C. Graphene-Based Photothermal Agent for Rapid and Effective Killing of Bacteria. *ACS Nano* **2013**, *7*, 1281−1290.
(13) Kholmanov, I. N.; Stoller, M. D.; Edgeworth, J.; Lee, W. H.; Li, H.; Lee, J.; Barnhart, C.; Potts, J. R.; Piner, R.; Akinwande, D.; Barrick, J. E.; Ruoff, R. S. Nanostructured Hybrid Transparent Conductive Films with Antibacterial Properties. *ACS Nano* **2012**, *6*, 5157−5163.
(14) Liu, S.; Zeng, T. H.; Hofmann, M.; Burcombe, E.; Wei, J.; Jiang, R.; Kong, J.; Chen, Y. Antibacterial Activity of Graphite, Graphite Oxide, Graphene Oxide, and Reduced Graphene Oxide: Membrane and Oxidative Stress. *ACS Nano* **2011**, *5*, 6971−6980.
(15) Loo, A. E. K.; Wong, Y. T.; Ho, R.; Wasser, M.; Du, T.; Ng, W. T.; Halliwell, B. Effects of Hydrogen Peroxide on Wound Healing in Mice in Relation to Oxidative Damage. *PLoS One* **2012**, *7*, e49215.
(16) Hayashi, E.; Mokudai, T.; Yamada, Y.; Nakamura, K.; Kanno, T.; Sasaki, K.; Niwano, Y. In Vitro and in Vivo Anti-Staphylococcus Aureus Activities of a New Disinfection System Utilizing Photolysis of Hydrogen Peroxide. *J. Biosci. Bioeng.* **2012**, *114*, 193−197.
(17) Murdoch, L. E.; Bailey, L.; Banham, E.; Watson, F.; Adams, N. M.; Chewins, J. Evaluating Different Concentrations of Hydrogen Peroxide in an Automated Room Disinfection System. *Lett. Appl. Microbiol.* **2016**, *63*, 178−182.
(18) Vatansever, F.; de Melo, W. C.; Avci, P.; Vecchio, D.; Sadasivam, M.; Gupta, A.; Chandran, R.; Karimi, M.; Parizotto, N. A.; Yin, R.; Tegos, G. P.; Hamblin, M. R. Antimicrobial Strategies Centered Around Reactive Oxygen Species–Bactericidal Antibiotics, Photodynamic Therapy, and Beyond. *FEMS Microbiol. Rev.* **2013**, *37*, 955−989.
(19) Walling, C. Fenton's Reagent Revisited. *Acc. Chem. Res.* **1975**, *8*, 125−131.
(20) Fenton, H. J. H. Lxxiii.-Oxidation of Tartaric Acid in Presence of Iron. *J. Chem. Soc., Trans.* **1894**, *65*, 899−910.
(21) Hayyan, M.; Hashim, M. A.; AlNashef, I. M. Superoxide Ion: Generation and Chemical Implications. *Chem. Rev.* **2016**, *116*, 3029−3085.
(22) Nahon, P.; Sutton, A.; Rufat, P.; Ziol, M.; Akouche, H.; Laguillier, C.; Charnaux, N.; Ganne-Carrie, N.; Grando-Lemaire, V.; N'Kontchou, G.; Trinchet, J. C.; Gattegno, L.; Pessayre, D.; Beaugrand, M. Myeloperoxidase and Superoxide Dismutase 2 Polymorphisms Comodulate the Risk of Hepatocellular Carcinoma and Death in Alcoholic Cirrhosis. *Hepatology* **2009**, *50*, 1484−1493.
(23) Gębicka, L.; Gębicki, J. L. Modification of Horseradish Peroxidase Induced by Hydroxyl Radicals. The Influence of Oxygen. *Biochimie* **1996**, *78*, 62−65.
(24) Martins, D.; Titorenko, V. I.; English, A. M. Cells with Impaired Mitochondrial H2O2 Sensing Generate Less *OH Radicals and Live Longer. *Antioxid. Redox Signaling* **2014**, *21*, 1490−1503.
(25) Sun, H.; Gao, N.; Dong, K.; Ren, J.; Qu, X. Graphene Quantum Dots-Band-Aids Used for Wound Disinfection. *ACS Nano* **2014**, *8*, 6202−6210.
(26) Wang, Z.; Dong, K.; Liu, Z.; Zhang, Y.; Chen, Z.; Sun, H.; Ren, J.; Qu, X. Activation of Biologically Relevant Levels of Reactive Oxygen Species by Au/g-C3N4 Hybrid Nanozyme for Bacteria Killing and Wound Disinfection. *Biomaterials* **2017**, *113*, 145−157.
(27) Gao, L.; Giglio, K. M.; Nelson, J. L.; Sondermann, H.; Travis, A. J. Ferromagnetic Nanoparticles with Peroxidase-Like Activity Enhance the Cleavage of Biological Macromolecules for Biofilm Elimination. *Nanoscale* **2014**, *6*, 2588−2593.
(28) Ivankovic, S.; Music, S.; Gotic, M.; Ljubesic, N. Cytotoxicity of Nanosize V(2)O(5) Particles to Selected Fibroblast and Tumor Cells. *Toxicol. In Vitro* **2006**, *20*, 286−294.
(29) Yang, J. F.; Zhou, S. B.; Xiao, A. G.; Li, W. J.; Ying, G. G. Chemical Oxidation of Sulfadiazine by the Fenton Process: Kinetics, Pathways, Toxicity Evaluation. *J. Environ. Sci. Health, Part B* **2014**, *49*, 909−916.
(30) Zhou, W.; Saran, R.; Liu, J. Metal Sensing by DNA. *Chem. Rev.* **2017**, *117*, 8272−8325.
(31) Liu, J.; Lu, Y. A Colorimetric Lead Biosensor Using DNAzyme-Directed Assembly of Gold Nanoparticles. *J. Am. Chem. Soc.* **2003**, *125*, 6642−6643.
(32) Liu, J.; Cao, Z.; Lu, Y. Functional Nucleic Acid Sensors. *Chem. Rev.* **2009**, *109*, 1948−1998.
(33) Li, Y.; Sen, D. Toward an Efficient DNAzyme. *Biochemistry* **1997**, *36*, 5589−5599.
(34) Kosman, J.; Juskowiak, B. Peroxidase-Mimicking DNAzymes for Biosensing Applications: a Review. *Anal. Chim. Acta* **2011**, *707*, 7−17.
(35) Stefan, L.; Denat, F.; Monchaud, D. Insights into How Nucleotide Supplements Enhance the Peroxidase-Mimicking DNAzyme Activity of the G-Quadruplex/Hemin System. *Nucleic Acids Res.* **2012**, *40*, 8759−8772.
(36) Ma, D. L.; Zhang, Z.; Wang, M.; Lu, L.; Zhong, H. J.; Leung, C. H. Recent Developments in G-Quadruplex Probes. *Chem. Biol.* **2015**, *22*, 812−828.
(37) Gribas, A. V.; Zhao, S.; Sakharov, I. Y. Improved Method for Chemiluminescent Determination of Peroxidase-Mimicking DNAzyme Activity. *Anal. Biochem.* **2014**, *466*, 19−23.
(38) Zhang, L.; Er, J. C.; Li, X.; Heng, J. J.; Samanta, A.; Chang, Y. T.; Lee, C. L. Development of Fluorescent Probes Specific for Parallel-Stranded G-Quadruplexes by a Library Approach. *Chem. Commun. (Cambridge, U. K.)* **2015**, *51*, 7386−7389.
(39) Tan, X.; Wang, Y.; Armitage, B. A.; Bruchez, M. P. Label-Free Molecular Beacons for Biomolecular Detection. *Anal. Chem.* **2014**, *86*, 10864−10869.
(40) Li, T.; Dong, S.; Wang, E. Label-Free Colorimetric Detection Of Aqueous Mercury Ion (Hg2+) Using Hg2+-Modulated G-Quadruplex-Based DNAzymes. *Anal. Chem.* **2009**, *81*, 2144−2149.
(41) Zhao, M.; Liao, N.; Zhuo, Y.; Chai, Y. Q.; Wang, J. P.; Yuan, R. Triple Quenching of a Novel Self-Enhanced Ru(II) Complex by Hemin/G-Quadruplex DNAzymes and Its Potential Application to Quantitative Protein Detection. *Anal. Chem.* **2015**, *87*, 7602−7609.
(42) Cheng, X.; Liu, X.; Bing, T.; Cao, Z.; Shangguan, D. General Peroxidase Activity of G-Quadruplex-Hemin Complexes and Its Application in Ligand Screening. *Biochemistry* **2009**, *48*, 7817−7823.
(43) Yang, X.; Fang, C.; Mei, H.; Chang, T.; Cao, Z.; Shangguan, D. Characterization of G-Quadruplex/Hemin Peroxidase: Substrate Specificity and Inactivation Kinetics. *Chem. - Eur. J.* **2011**, *17*, 14475−14484.
(44) Zhang, Z.; Liu, J. Intracellular Delivery of a Molecularly Imprinted Peroxidase Mimicking DNAzyme for Selective Oxidation. *Mater. Horiz.* **2018**, *5*, 738−744.
(45) Yaku, H.; Murashima, T.; Miyoshi, D.; Sugimoto, N. Specific Binding of Anionic Porphyrin and Phthalocyanine to the G-Quadruplex with a Variety of in Vitro and in Vivo Applications. *Molecules* **2012**, *17*, 10586−10613.

DOI: 10.1021/acsabm.8b00211
ACS Appl. Bio Mater. 2018, 1, 1019−1027

(46) Li, J.; Zheng, W.; Kwon, A. H.; Lu, Y. In Vitro Selection and Characterization of a Highly Efficient Zn(II)-Dependent RNA-Cleaving Deoxyribozyme. *Nucleic Acids Res.* **2000**, *28*, 481−488.
(47) Yuan, K.; Xie, K.; Fox, J.; Zeng, H.; Gao, H.; Huang, C.; Wu, M. Decreased Levels of miR-224 and the Passenger Strand of miR-221 Increase MBD2, Suppressing Maspin and Promoting Colorectal Tumor Growth and Metastasis in Mice. *Gastroenterology* **2013**, *145*, 853−864.
(48) Zhu, L.; Li, C.; Zhu, Z.; Liu, D.; Zou, Y.; Wang, C.; Fu, H.; Yang, C. J. In Vitro Selection of Highly Efficient G-Quadruplex-Based DNAzymes. *Anal. Chem.* **2012**, *84*, 8383−8390.
(49) Li, X.; He, S.; Zhou, X.; Ye, Y.; Tan, S.; Zhang, S.; Li, R.; Yu, M.; Jundt, M. C.; Hidebrand, A.; Wang, Y.; Li, G.; Huang, C.; Wu, M. Lyn Delivers Bacteria to Lysosomes for Eradication through TLR2-Initiated Autophagy Related Phagocytosis. *PLoS Pathog.* **2016**, *12*, e1005363.
(50) Li, X.; He, S.; Li, R.; Zhou, X.; Zhang, S.; Yu, M.; Ye, Y.; Wang, Y.; Huang, C.; Wu, M. Pseudomonas Aeruginosa Infection Augments Inflammation through miR-301b Repression of c-Myb-Mediated Immune Activation and Infiltration. *Nat. Microbiol.* **2016**, *1*, 16132.
(51) Guo, Q.; Shen, N.; Yuan, K.; Li, J.; Wu, H.; Zeng, Y.; Fox, J., 3rd; Bansal, A. K.; Singh, B. B.; Gao, H.; Wu, M. Caveolin-1 Plays a Critical Role in Host Immunity Against Klebsiella Pneumoniae by Regulating STAT5 and Akt Activity. *Eur. J. Immunol.* **2012**, *42*, 1500−1511.
(52) Kannan, S.; Pang, H.; Foster, D. C.; Rao, Z.; Wu, M. Human 8-Oxoguanine DNA Glycosylase Increases Resistance to Hyperoxic Cytotoxicity in Lung Epithelial Cells and Involvement with Altered MAPK Activity. *Cell Death Differ.* **2006**, *13*, 311−323.
(53) He, S.; Li, X.; Li, R.; Fang, L.; Sun, L.; Wang, Y.; Wu, M. Annexin A2Modulates ROS and Impacts Inflammatory Response via IL-17 Signaling in Polymicrobial Sepsis Mice. *PLoS Pathog.* **2016**, *12*, e1005743.
(54) Cai, N.; Li, Y.; Chen, S.; Su, X. A Fluorometric Assay Platform for Caffeic Acid Detection Based on the G-Quadruplex/Hemin DNAzyme. *Analyst* **2016**, *141*, 4456−4462.
(55) Isaksen, I. S. A.; Dalsøren, S. B. Getting a Better Estimate of an Atmospheric Radical. *Science* **2011**, *331*, 38−39.
(56) Fontmorin, J. M.; Burgos Castillo, R. C.; Tang, W. Z.; Sillanpaa, M. Stability of 5,5-Dimethyl-1-Pyrroline-N-Oxide as a Spin-Trap for Quantification of Hydroxyl Radicals in Processes Based on Fenton Reaction. *Water Res.* **2016**, *99*, 24−32.
(57) Azman, N. A. M.; Peiró, S.; Fajarí, L.; Julià, L.; Almajano, M. P. Radical Scavenging of White Tea and Its Flavonoid Constituents by Electron Paramagnetic Resonance (EPR) Spectroscopy. *J. Agric. Food Chem.* **2014**, *62*, 5743−5748.
(58) Hayashi, E.; Mokudai, T.; Yamada, Y.; Nakamura, K.; Kanno, T.; Sasaki, K.; Niwano, Y. In Vitro and in Vivo Anti-Staphylococcus Aureus Activities of a New Disinfection System Utilizing Photolysis of Hydrogen Peroxide. *J. Biosci. Bioeng.* **2012**, *114*, 193−197.
(59) Ishibashi, K. i.; Fujishima, A.; Watanabe, T.; Hashimoto, K. Detection of Active Oxidative Species in TiO2 Photocatalysis Using the Fluorescence Technique. *Electrochem. Commun.* **2000**, *2*, 207−210.
(60) Ge, S.; Liu, F.; Liu, W.; Yan, M.; Song, X.; Yu, J. Colorimetric Assay of K-562 Cells Based on Folic Acid-Conjugated Porous Bimetallic Pd@Au Nanoparticles for Point-of-Care Testing. *Chem. Commun.* **2014**, *50*, 475−477.
(61) Guo, Y.; Chen, J.; Cheng, M.; Monchaud, D.; Zhou, J.; Ju, H. A Thermophilic Tetramolecular G-Quadruplex/Hemin DNAzyme. *Angew. Chem., Int. Ed.* **2017**, *56*, 16636−16640.
(62) Stefan, L.; Denat, F.; Monchaud, D. Deciphering the DNAzyme Activity of Multimeric Quadruplexes: Insights into Their Actual Role in the Telomerase Activity Evaluation Assay. *J. Am. Chem. Soc.* **2011**, *133*, 20405−20415.
(63) Ye, Y.; Lin, P.; Zhang, W.; Tan, S.; Zhou, X.; Li, R.; Pu, Q.; Koff, J. L.; Dhasarathy, A.; Ma, F.; Deng, X.; Jiang, J.; Wu, M. DNA Repair Interacts with Autophagy to Regulate Inflammatory Responses to Pulmonary Hyperoxia. *J. Immunol.* **2017**, *198*, 2844−2853.
(64) Wang, K.; Zhang, T.; Lei, Y.; Li, X.; Jiang, J.; Lan, J.; Liu, Y.; Chen, H.; Gao, W.; Xie, N.; Chen, Q.; Zhu, X.; Liu, X.; Xie, K.; Peng, Y.; Nice, E. C.; Wu, M.; Huang, C.; Wei, Y. Identification of ANXA2 (Annexin A2) as a Specific Bleomycin Target to Induce Pulmonary Fibrosis by Impeding TFEB-Mediated Autophagic Flux. *Autophagy* **2018**, *14*, 269−282.
(65) Li, L. L.; Wang, H. Antibacterial Agents: Enzyme-Coated Mesoporous Silica Nanoparticles as Efficient Antibacterial Agents in Vivo. *Adv. Healthcare Mater.* **2013**, *2*, 1298−1298.
(66) Kumar, S.; Bandyopadhyay, U. Free Heme Toxicity and Its Detoxification Systems in Human. *Toxicol. Lett.* **2005**, *157*, 175−188.
(67) Chen-Roetling, J.; Benvenisti-Zarom, L.; Regan, R. F. Cultured Astrocytes From Heme Oxygenase-1 Knockout Mice Are More Vulnerable to Heme-Mediated Oxidative Injury. *J. Neurosci. Res.* **2005**, *82*, 802−810.

DOI: 10.1021/acsabm.8b00211
ACS Appl. Bio Mater. 2018, 1, 1019−1027